Quantum-mechanical picture of peripheral chiral dynamics

C. Granados and C. Weiss

Quantum–mechanical picture of peripheral chiral dynamics

C. Granados[1] and C. Weiss[2]

[1]*Department of Physics and Astronomy, Nuclear Physics, Uppsala University, 75120 Uppsala, Sweden*
[2]*Theory Center, Jefferson Lab, Newport News, VA 23606, USA*

The nucleon's peripheral transverse charge and magnetization densities are computed in chiral effective field theory. The densities are represented in first–quantized form, as overlap integrals of chiral light–front wave functions describing the transition of the nucleon to soft pion–nucleon intermediate states. The orbital motion of the pion causes a large left–right asymmetry in a transversely polarized nucleon. The effect attests to the relativistic nature of chiral dynamics [pion momenta $k = O(M_\pi)$] and could be observed in form factor measurements at low momentum transfer.

I. INTRODUCTION

The long–distance behavior of strong interactions is governed by the spontaneous breaking of chiral symmetry in the microscopic theory of Quantum Chromodynamics. The associated Goldstone bosons — the pions — are almost massless on the hadronic scale, couple weakly to other hadrons (proportional to their momentum), and mediate long–distance interactions. The resulting "chiral dynamics" can be studied systematically using methods of effective field theory (EFT) [1, 2] and explains numerous phenomena in low–energy pion–pion and pion–nucleon scattering, the nucleon–nucleon interaction at large distances, and electroweak interactions of hadrons.

Chiral dynamics represents an essentially relativistic dynamical system, as the pion 4–momenta in typical processes are of the order of the pion mass, $k = O(M_\pi)$ [1], and the number of particles changes due to quantum fluctuations. Chiral EFT is therefore usually formulated and solved as a second–quantized field theory. While this allows one to calculate most observables of interest, for many purposes it would be desirable to have a first–quantized, particle–based formulation of the dynamics. It would make it possible to follow the space–time evolution of chiral processes and gain a more intuitive understanding of their effects. It would introduce the concept of a wave function and its densities and help quantify the spatial structure of hadrons, the orbital motion of pions, and polarization effects.

The light–front (LF) formulation of relativistic dynamics [3–5] makes it possible to construct a consistent first–quantized description of essentially relativistic systems. In this framework one follows the evolution of the system in LF time $x^+ = x^0 + x^3 \equiv t + z$. The wave functions at fixed x^+ are invariant under Lorentz boosts in the longitudinal ($z-$) direction, so that their particle content and densities are frame–independent and have objective meaning — in contrast to the equal–time wave function, where they are frame–dependent. Transverse boosts (in the x, y–plane) are kinematical and preserve the particle number. Orbital motion and spin are naturally expressed and lead to a description in close correspondence to non-relativistic quantum mechanics [5].

In this work we use chiral EFT in the LF formulation to study the long–distance contributions to the nucleon's electromagnetic current matrix element and explain their properties. The form factors are expressed in terms of the transverse densities of charge and magnetization at fixed LF time [6–9]. At peripheral transverse distances $b = O(M_\pi^{-1})$ the isovector densities have been calculated using chiral EFT in the leading–order (LO) approximation [10]. We represent them here in first–quantized form, as overlap integrals of chiral LF wave functions describing the transition of the nucleon to soft pion–nucleon intermediate states. The new representation leads to a simple quantum–mechanical picture, according to which the orbital motion of the soft pion causes a left-right asymmetry of the "plus" current density in a transversely polarized nucleon [8]. The effect is sizable and attests to the essentially relativistic nature of chiral dynamics.

II. TRANSVERSE DENSITIES

The transition matrix element of the electromagnetic current between nucleon states with 4–momenta p_1 and p_2 is parametrized by the Dirac and Pauli form factors, $F_1(t)$ and $F_2(t)$, which are functions of the invariant momentum transfer $t \equiv \Delta^2 = (p_2 - p_1)^2$ (we follow the notation of Ref. [10]). In a frame where the momentum transfer is transverse, $\boldsymbol{\Delta}_T \equiv (\Delta^x, \Delta^y) \neq 0$, $\Delta^0 = \Delta^z = 0$, the form factors are represented as a Fourier integral over a transverse coordinate $\boldsymbol{b} \equiv (b^x, b^y)$ [7, 9]

$$F_{1,2}(t = -\boldsymbol{\Delta}_T^2) = \int d^2b \, e^{i\boldsymbol{\Delta}_T \cdot \boldsymbol{b}} \, \rho_{1,2}(b). \quad (1)$$

The functions $\rho_{1,2}(b \equiv |\boldsymbol{b}|)$ describe the transverse spatial distribution of charge and magnetization in the nucleon at fixed LF time. Specifically, in a state where the nucleon is localized in transverse space at the origin, and spin–polarized in the y–direction, the expectation value of the current $J^+ \equiv J^0 + J^3$ at LF time $x^+ = 0$ and transverse position $\boldsymbol{x}_T = \boldsymbol{b}$ is

$$\langle J^+(\boldsymbol{b}) \rangle_{\text{loc}} = (...)[\rho_1(b) + (2S^y) \cos\phi \, \widetilde{\rho}_2(b)], \quad (2)$$
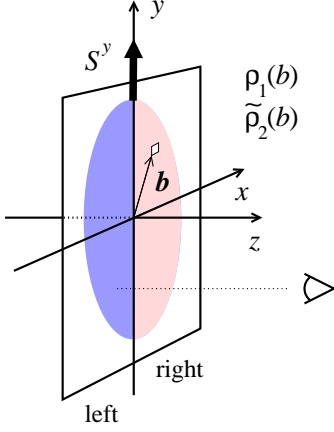
FIG. 1. (Color online) Interpretation of the transverse densities in a nucleon state polarized in the y–direction, Eq. (2).

$$\widetilde{\rho}_2(b) \equiv \frac{\partial}{\partial b}\left[\frac{\rho_2(b)}{2M_N}\right], \tag{3}$$

where (...) hides a trivial factor arising from the normalization of states, $\cos\phi \equiv b^x/b$, and $S^y = \pm 1/2$ is the y–spin projection in the nucleon rest frame (see Fig. 1) [7, 10]. Thus $\rho_1(b)$ describes the spin–independent (left–right symmetric) and $\cos\phi\,\widetilde{\rho}_2(b)$ the spin–dependent (left–right antisymmetric) plus current in the y–polarized nucleon. Choosing $S^y = +1/2$ and looking at two opposite points on the x–axis, $\boldsymbol{b} = \mp b\boldsymbol{e}_x$, one has

$$\langle J^+(\mp b\boldsymbol{e}_x)\rangle_{\text{loc}} = (...)\,[\rho_1(b) \mp \widetilde{\rho}_2(b)]$$
$$\equiv (...)\,\rho_{\text{left/right}}(b), \tag{4}$$

which shows that $\rho_1(b)$ and $\widetilde{\rho}_2(b)$ can be determined directly as the left–right symmetric and antisymmetric parts of the plus current on the x–axis.

III. CHIRAL PERIPHERY

At peripheral distances $b = O(M_\pi^{-1})$ the transverse densities are governed by chiral dynamics and can be computed from first principles using chiral EFT [10, 11]. The densities can be obtained from the relativistic chiral EFT results for the form factors [12–17]. Peripheral contributions arise from the chiral processes in which the current couples to the nucleon through two–pion exchange, i.e., contributions to the two–pion cut of the isovector form factors at $t > 4M_\pi^2$. At LO these are given by the Feynman diagrams of Fig. 2a, where the vertices are those of the relativistic chiral Lagrangian [18]; the densities depend only on the imaginary parts of the form factors on the physical cut [10, 11] and are not sensitive to the choice of relativistic renormalization scheme at LO (for a review of the schemes and their properties, see Ref. [16]). The first diagram contains a term in which the pole of the intermediate nucleon propagator is canceled
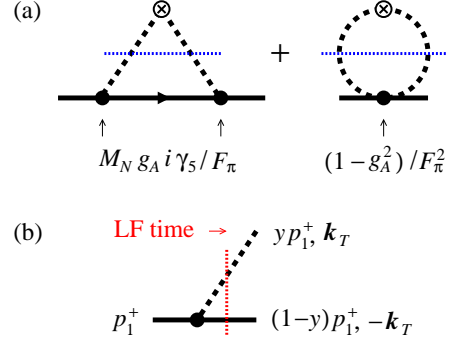

FIG. 2. (Color online) (a) Feynman diagrams of LO chiral EFT processes contributing to the peripheral transverse densities (two–pion cut of the form factors). Indicated below are the effective vertices obtained after isolating the nucleon pole term of the first diagram. (b) Chiral LF wave function of the nucleon.

by the numerator; this term is of the same form as the contact term from the second diagram and can be combined with it. Effectively this amounts to replacing the πNN vertices in the first diagram by the pseudoscalar vertex $M_N g_A i\gamma_5/F_\pi$, and changing the $\pi\pi NN$ contact coupling in the second as $1/F_\pi^2 \to (1 - g_A^2)/F_\pi^2$, as indicated in Fig. 2a [10, 11]. With this rearrangement the first Feynman diagram is given entirely by the nucleon pole contribution. It can therefore be represented as a LF time–ordered process in which the initial nucleon makes a transition to a soft pion–nucleon intermediate state and back. The transition is described by the chiral LF wave function (Fig. 2b)

$$\Psi(y, \boldsymbol{k}_T; \text{pol}) \equiv \frac{\Gamma(y, \boldsymbol{k}_T; \text{pol})}{\Delta\mathcal{M}^2(y, \boldsymbol{k}_T)}, \tag{5}$$

where $y = k^+/p_1^+$ is the LF plus momentum fraction of the pion, $\boldsymbol{k}_T$ its transverse momentum relative to the initial nucleon with $\boldsymbol{p}_{1T} = 0$, and "pol" denotes generic spin quantum numbers characterizing the initial and intermediate nucleon states. In the numerator, Γ is the on-shell pseudoscalar πNN vertex between the initial nucleon spinor and the intermediate one with LF momentum $(1 - y)p_1^+$ and $-\boldsymbol{k}_T$,

$$\Gamma(y, \boldsymbol{k}_T; \text{pol}) \equiv \frac{g_A M_N}{F_\pi}\,\bar{u}((1-y)p_1^+, -\boldsymbol{k}_T)$$
$$\times\, i\gamma_5\, u(p_1^+, \boldsymbol{0}_T). \tag{6}$$

Its form is unambiguously determined by the rearrangement of the EFT interactions; the peripheral densities are insensitive to the off-shell behavior [19]. In the denominator of Eq. (5) $\Delta\mathcal{M}^2$ denotes the invariant mass difference between the initial and intermediate state,

$$\Delta\mathcal{M}^2(y, \boldsymbol{k}_T) \equiv [\boldsymbol{k}_T^2 + M_T^2(y)]/[y(1-y)], \tag{7}$$
$$M_T^2(y) \equiv (1-y)M_\pi^2 + y^2 M_N^2, \tag{8}$$

which is proportional to the LF energy denominator of the transition [5]. The wave function for a state moving with overall transverse momentum $\boldsymbol{p}_{1T} \neq 0$ is obtained by a transverse boost, and analogous formulas describe the transition back to the final state with $\boldsymbol{p}_{2T}$. The chiral wave functions refer to the parametric regime $|\boldsymbol{k}_T| = O(M_\pi)$ and $y = O(M_\pi/M_N)$, where the pion is soft and couples weakly to the nucleon, and are used in this context only. The coordinate–space wave function is

$$\Phi(y, \boldsymbol{r}_T, \text{pol}) \equiv \int \frac{d^2 k_T}{(2\pi)^2} \, e^{i\boldsymbol{k}_T \cdot \boldsymbol{r}_T} \, \Psi(y, \boldsymbol{k}_T; \text{pol}), \quad (9)$$

where $\boldsymbol{r}_T$ is the transverse separation of the pion–nucleon system in the intermediate state and $|\boldsymbol{r}_T| = O(M_\pi^{-1})$.

The peripheral transverse densities can be expressed as overlap integrals of the chiral LF wave functions of the initial and final nucleon and an effective contact term. A particularly simple form is obtained when the nucleon spin states in the wave function are quantized in the transverse y–direction. Transversely polarized LF spinors are constructed by preparing a transverse spinor in the nucleon rest frame and performing a longitudinal and a transverse boost to get to the desired LF momentum [5]. We denote the LF wave function Eq. (9) defined with such transversely polarized nucleon spin states by

$$\Phi_{\text{tr}}(y, \boldsymbol{r}_T; \tau, \tau_1), \quad (10)$$

where τ_1 and τ are the y–spin projections of the initial and the intermediate nucleon states; the complex conjugate function $\Phi_{\text{tr}}^*(y, \boldsymbol{r}_T; \tau, \tau_2)$ describes the transition back to the final state with y–spin τ_2. At the special points $\boldsymbol{b} = \mp b\boldsymbol{e}_x$ [cf. Eq. (4)] only the transverse spin–flip wave function ($\tau_1 = \tau_2 = +1/2, \tau = -1/2$) contributes to the current matrix element; the spin–nonflip wave function ($\tau = +1/2$) vanishes on the transverse x–axis. We obtain the isovector densities as $[\rho^V \equiv (\rho^p - \rho^n)/2]$

$$\left.\begin{array}{c} \rho_{\text{left}}^V(b) \\ \rho_{\text{right}}^V(b) \end{array}\right\} = \int_0^1 dy \, \frac{|\Phi_{\text{tr}}(y, \mp r_T \boldsymbol{e}_x; -\frac{1}{2}, \frac{1}{2})|^2}{2\pi y (1-y)^3}$$
$$[r_T = b/(1-y)]. \quad (11)$$

The coordinate–space wave function is readily obtained by deriving the explicit form of the vertex function Eq. (6) for transversely polarized LF spinors, $\Gamma_{\text{tr}}(y, \boldsymbol{k}_T; \tau, \tau_1)$, with $\tau_1 = +1/2$ and $\tau = -1/2$,

$$\Gamma_{\text{tr}}(y, \boldsymbol{k}_T; -\tfrac{1}{2}, \tfrac{1}{2}) = \frac{g_A M_N (y M_N + i k^x)}{F_\pi \sqrt{1-y}}, \quad (12)$$

inserting it in Eq. (5), and evaluating the Fourier integral Eq. (9). The approximate expressions for the spin–flip wave function at large separations $r_T \gg M_T^{-1}$ are

$$\Phi_{\text{tr}}(y, \mp r_T \boldsymbol{e}_x; -\tfrac{1}{2}, \tfrac{1}{2})$$
$$= \frac{g_A M_N \, y \sqrt{1-y}}{2\sqrt{2\pi} F_\pi} \, [y M_N \pm M_T(y)] \, \frac{e^{-M_T(y) r_T}}{\sqrt{M_T(y) r_T}}; \quad (13)$$
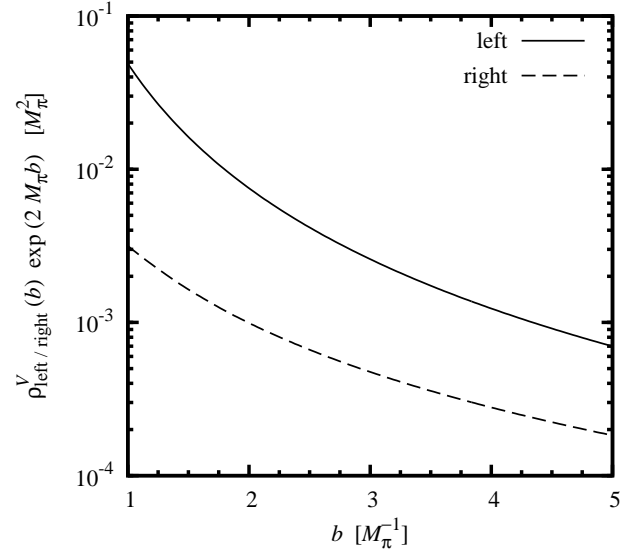

FIG. 3. Left and right peripheral transverse densities in LO chiral EFT, as given by Eq. (11) and the contact term. The plot shows the densities after extraction of the exponential factor $\exp(-2M_\pi b)$. The transverse distance b and the densities are given in units of the pion mass.

the exact expressions for any r_T involve modified Bessel functions. The charge and magnetization densities are then obtained as

$$\left.\begin{array}{c} \rho_1^V(b) \\ \widetilde{\rho}_2^V(b) \end{array}\right\} = \frac{1}{2}[\pm\rho_{\text{left}}^V(b) + \rho_{\text{right}}^V(b)]. \quad (14)$$

The effective contact term in Fig. 2 describes the instantaneous contributions to the current in LF time (zero modes) and has to be added to Eq. (11). The coupling $\propto (1 - g_A^2)$ shows that this term reflects the nucleon's internal structure due to non-chiral intermediate states [10]. Its contribution to the density is left–right symmetric and amounts to <10% of $\rho_1^V(b)$ at $b > 1\, M_\pi^{-1}$. The peripheral densities are thus practically determined by the wave function overlap Eq. (11).

The LF representation Eq. (11) (including the contact term) is *exactly equivalent* to the result of the relativistically invariant EFT calculation [10] and embodies the entire chiral structure of the peripheral densities at LO. It reveals several interesting properties: (a) The left and right densities are of the same parametric order in the heavy–baryon limit, $\rho_{\text{left}}^V(b)/\rho_{\text{right}}^V(b) = O(1)$ for $M_\pi/M_N \to 0$, because the integral in Eq. (11) is dominated by pion momentum fractions $y = O(M_\pi/M_N)$. (b) The left and right densities in Eq. (11) are individually positive, $\rho_{\text{left/right}}^V(b) > 0$. The charge and magnetization densities Eq. (14) therefore obey an inequality,

$$|\widetilde{\rho}_2^V(b)| < \rho_1^V(b), \quad (15)$$

as was observed numerically in Ref. [10]. (c) The left–right asymmetry of the densities produced by chiral dy-

namics is numerically large (see Fig. 3). The ratio $\rho_{\text{left}}^V(b)/\rho_{\text{right}}^V(b)$ is ~ 10 at $b = 1 M_\pi^{-1}$ and decreases slowly at larger distances. As a result the charge and magnetization densities Eq. (14) are almost equal and opposite,

$$\widetilde{\rho}_2^V(b) \approx -\rho_1^V(b), \tag{16}$$

and the inequality Eq. (15) is almost saturated.

IV. QUANTUM-MECHANICAL PICTURE

Our findings can be summarized in a simple quantum–mechanical picture of the peripheral transverse densities in chiral EFT (see Fig. 4), inspired by the general arguments of Ref. [8]. Consider a physical proton with y–spin projection $+1/2$ in the rest frame. In the interaction picture we may think of this system as a bare nucleon that undergoes transitions to multiple pion–nucleon states through the chiral EFT interactions. In LO the peripheral left/right densities (at the points $\bm{b} = \mp b \bm{e}_x$) arise from the single $\pi^+ n$ intermediate state, in which the neutron has y–spin $-1/2$ and the pion is in a state with orbital angular momentum $L = 1$ and y–projection $L^y = +1$. Because of the orbital motion the pion on the left moves toward the observer and has net positive z–momentum $k^z > 0$, while the pion on the right moves away and has $k^z < 0$. The plus current carried by a free charged pion is $\langle \pi^+(k)|J^+|\pi^+(k)\rangle = 2k^+ = 2(\sqrt{|\bm{k}|^2 + M_\pi^2} + k^z)$. The observer thus sees a larger plus current on the left than on the right, resulting in a left–right asymmetry. If the motion of the pion were non-relativistic, $|\bm{k}| \ll M_\pi$ the asymmetry would be small, $\rho_{\text{left}}/\rho_{\text{right}} = 1 + O(|\bm{k}|/M_\pi)$. That the asymmetry obtained in chiral EFT is large therefore directly attests to relativistic motion of the pion, $|\bm{k}| = O(M_\pi)$.

The intuitive arguments presented here assume rotational symmetry around the y–axis, which is not present in the LF formulation. The explicit expressions Eqs. (13) and (14) show, however, that all the described features are realized in the LF formulation as well, if the nucleon transverse spin states are defined as specified above.

V. SUMMARY AND DISCUSSION

The LF formulation of chiral EFT provides a concise representation of the peripheral transverse densities, which reveals new properties (positivity, inequality) and permits a simple mechanical interpretation. The large left–right asymmetry is rooted in the spin structure of the pion–nucleon coupling and the essentially relativistic motion of pions and represents a striking chiral effect. It could be observed by extracting the peripheral transverse densities from precise measurements of the nucleon's Dirac and Pauli form factors at low momentum transfer, using dispersion fits that respect the analytic properties [20]; see Ref. [21] for details. Similar chiral
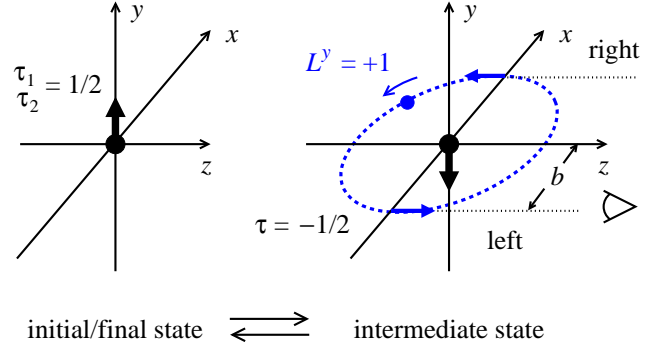

FIG. 4. (Color online) Quantum–mechanical picture of chiral dynamics in the peripheral transverse densities (explanation in text).

left–right asymmetries may be observed in high-energy proton–proton collisions, by selecting events in which the scattering takes place on a peripheral pion; such processes would permit much more direct tests of the effect described here.

The present study focuses on the structure of the peripheral transverse densities in LO chiral EFT. The relativistic LO approximation captures the basic asymptotic behavior of the densities in the chiral region $b = O(M_\pi^{-1})$, as established on general grounds [10, 11]. It correctly implements the analytic properties of the form factors in the region $t = O(M_\pi^2)$ — the two–pion cut at $t > 4M_\pi^2$, and the enhancement of the imaginary parts due to a subthreshold singularity on the unphysical sheet — which govern the form of the large–distance behavior of the densities. The densities are obtained from the imaginary parts of the form factors on the cut, which are renormalization–scheme–independent in LO. Higher–order chiral corrections modify the coupling of the two–pion exchange to the electromagnetic current and to the nucleon, but not the analytic properties at $t = O(M_\pi^2)$, and thus do not qualitatively change the asymptotic behavior at $b = O(M_\pi^{-1})$. A numerical estimate, using the higher–order chiral EFT results for $\text{Im}\, F_{1,2}^V(t)$ at $t > 4M_\pi^2$ of Ref. [15] and the dispersive representation of transverse densities of Refs. [10, 11], indicates that at $b = 2\, M_\pi^{-1}$ higher–order chiral corrections would increase $\rho_1^V(b)$ by a factor ~ 1.1 and $\widetilde{\rho}_2^V(b)$ by ~ 1.9; at $b = 5\, M_\pi^{-1}$ the factors are ~ 1.2 and ~ 1.5 respectively (note that this estimate is scheme–dependent and includes both higher–order loop corrections and contact terms [15]). The trend of the higher–order corrections would not change our conclusion regarding the large left–right asymmetry in the nucleon's peripheral plus current density. How such higher–order chiral corrections could be incorporated in the LF wave function representation described here, what renormalization scheme would be appropriate for this purpose, and how the corrections would be split between the wave function overlap and contact terms, are interesting questions that merit a dedicated future study.

The dispersive representation [10, 11] can also be used to evaluate the peripheral transverse densities with empirical estimates of $\mathrm{Im}\, F_{1,2}^{V}(t)$ at $t > 4M_\pi^2$ obtained from dispersion analysis [22, 23]. This approach allows one to combine the contributions to the densities from soft–pion exchange at $t = O(M_\pi^2)$ (which are captured by the chiral EFT calculation reported here) with those of ρ meson exchange at $t = O(M_\rho^2)$. Numerical studies show that the soft–pion contributions become significant only at $b \sim 2\, M_\pi^{-1}$ and account for the total isovector densities only at $b \gtrsim 3\, M_\pi^{-1}$ [21]. This defines the region of applicability of chiral EFT in the peripheral transverse densities.

The peripheral chiral structure described here appears in the isovector transverse densities. In the isoscalar combination $\rho^S \equiv (\rho^p + \rho^n)/2$ the chiral contributions involve three–pion exchange between the current and the nucleon and are strongly suppressed; these densities are generated mainly by non-chiral ω meson exchange up to very large distances [21]. As a consequence the isovector combination dominates at large b, and its chiral structure governs the behavior of the individual proton and neutron densities: $\rho^{p,n}(b) = \rho^S(b) \pm \rho^V(b) \approx \pm\rho^V(b)$ at $b \gtrsim 3\, M_\pi^{-1}$.

Further details regarding the LF wave function representation of peripheral transverse densities, including longitudinal spin and the correspondence with LF time-ordered perturbation theory, are presented in a recent article [24]. The representation can be extended to include intermediate Δ isobars and implement the proper scaling behavior in the large–N_c limit of QCD [10, 11]. It can also be used to compute the peripheral densities of matter and angular momentum (describing the form form factors of the energy–momentum tensor) and develop a mechanical representation of these structures. It can be applied further to the nucleon's peripheral parton densities (generalized parton distributions) [19, 25]. The LF representation has also been employed to study aspects of chiral nucleon structure (self–energies, electromagnetic couplings) without restriction to peripheral distances [26].

[1] J. Gasser and H. Leutwyler, Annals Phys. **158**, 142 (1984); Nucl. Phys. B **250**, 465 (1985).
[2] S. Weinberg, Phys. Lett. B **251**, 288 (1990); Nucl. Phys. B **363**, 3 (1991).
[3] P. A. M. Dirac, Rev. Mod. Phys. **21**, 392 (1949).
[4] H. Leutwyler and J. Stern, Annals Phys. **112**, 94 (1978).
[5] S. J. Brodsky, H.–C. Pauli and S. S. Pinsky, Phys. Rept. **301**, 299 (1998).
[6] D. E. Soper, Phys. Rev. D **15**, 1141 (1977).
[7] M. Burkardt, Phys. Rev. D **62**, 071503 (2000) [Erratum-ibid. D **66**, 119903 (2002)].
[8] M. Burkardt, Int. J. Mod. Phys. A **18**, 173 (2003).
[9] G. A. Miller, Phys. Rev. Lett. **99**, 112001 (2007); Ann. Rev. Nucl. Part. Sci. **60**, 1 (2010).
[10] C. Granados and C. Weiss, JHEP **1401**, 092 (2014).
[11] M. Strikman and C. Weiss, Phys. Rev. C **82**, 042201 (2010).
[12] J. Gasser, M. E. Sainio and A. Svarc, Nucl. Phys. B **307**, 779 (1988).
[13] V. Bernard, N. Kaiser, J. Kambor and U.–G. Meissner, Nucl. Phys. B **388**, 315 (1992).
[14] B. Kubis and U.–G. Meissner, Nucl. Phys. A **679**, 698 (2001).
[15] N. Kaiser, Phys. Rev. C **68** (2003) 025202.
[16] T. Ledwig, J. Martin-Camalich, V. Pascalutsa and M. Vanderhaeghen, Phys. Rev. D **85**, 034013 (2012).
[17] T. Bauer, J. C. Bernauer and S. Scherer, Phys. Rev. C **86**, 065206 (2012).
[18] T. Becher and H. Leutwyler, Eur. Phys. J. C **9**, 643 (1999).
[19] M. Strikman and C. Weiss, Phys. Rev. D **80**, 114029 (2009).
[20] M. A. Belushkin, H.–W. Hammer and U.–G. Meissner, Phys. Rev. C **75**, 035202 (2007). I. T. Lorenz, H.–W. Hammer and U.–G. Meissner, Eur. Phys. J. A **48**, 151 (2012).
[21] G. A. Miller, M. Strikman and C. Weiss, Phys. Rev. C **84**, 045205 (2011).
[22] G. Höhler *et al.*, Nucl. Phys. **B114**, 505 (1976).
[23] M. A. Belushkin, H. W. Hammer and U. G. Meissner, Phys. Lett. B **633**, 507 (2006).
[24] C. Granados and C. Weiss, JHEP **1507**, 170 (2015).
[25] M. Strikman and C. Weiss, Phys. Rev. D **69**, 054012 (2004);
[26] C.–R. Ji, W. Melnitchouk and A. W. Thomas, Phys. Rev. D **80**, 054018 (2009); Phys. Rev. D **88**, 076005 (2013). M. Burkardt, K. S. Hendricks, C.–R. Ji, W. Melnitchouk and A. W. Thomas, Phys. Rev. D **87**, 056009 (2013).